Available online at www.sciencedirect.com
SCIENCE DIRECT
Polymer 47 (2006) 3436–3447
polymer
www.elsevier.com/locate/polymer

Sequence distribution affect the phase behavior and hydrogen bonding strength in blends of poly(vinylphenol-*co*-methyl methacrylate) with poly(ethylene oxide)

Chen-Lung Lin, Wan-Chun Chen, Shiao-Wei Kuo *, Feng-Chih Chang

Institute of Applied Chemistry, National Chiao Tung University, Hsinchu 30050, Taiwan, ROC

Received 10 December 2005; received in revised form 14 March 2006; accepted 19 March 2006
Available online 3 April 2006

Abstract

Experimental results indicate that the PEO was miscible with PVPh-*r*-PMMA copolymers as shown by the existence of single composition-dependent glass transition temperature over the entire compositions. However, the PVPh-*b*-PMMA copolymer with PEO shows a like closed loop phase-separated region in this copolymer/homopolymer blend system. Furthermore, FTIR reveals that at least three competing equilibrium are present in these blends; self-association (hydroxyl–hydroxyl), interassociation (hydroxyl–carbonyl) of PVPh-*co*-PMMA, and hydroxyl–ether interassociation between PVPh and PEO. Based on the Painter–Coleman Association Model (PCAM), a value for inter-association, $K_C = 300$ is obtained in PVPh-*b*-PMMA/PEO blend system at room temperature. Although the relative ratio of interassociation equilibrium constant of PEO to PMMA is larger in PVPh-*b*-PMMA/PEO blend system, the PVPh-*r*-PMMA/PEO blend system has greater $\Delta\nu$ and greater homogeneity at the molecular scale than the PVPh-*b*-PMMA/PEO blend system because of the ΔK effect.

Keywords: Sequence distribution; Polymer blend; Hydrogen bonding.

1. Introduction

The miscibility of polymer blend has received much attention in polymer science. For macromolecules, the Gibbs free energy of mixing is mainly controlled by its enthalpic contribution because the entropic term is usually favorable but very small. Therefore, polymer pairs with complementary chemical structures favoring specific interactions (and, thus a negative enthalpy of mixing) usually lead to miscible systems [1–4]. Ideally, one polymer should possess donor sites and the other possesses acceptor sites on their respective chains. The most commonly observed interactions are of the acid–base type, i.e. hydrogen bonding [5], dipole–dipole, and charge-transfer interactions. On the contrary, when only dispersive forces can be expected between components, a positive (unfavorable) contribution of the enthalpic term is expected and as a consequence these systems are usually immiscible or phase-separated.

In order to obtain miscible polymer blends with desirable properties, it is very important to understand factors affecting the miscibility of polymer mixtures. The miscibility of copolymer/homopolymer blends has been successfully described by the binary interaction model [6–8]. According to this model, the mutual repulsive force between dissimilar segments in the copolymer can lead to negative heat of mixing necessary to attain miscibility. Paul et al. [9–11], Karasz et al. [12,13], and Jo et al. [14] have further extended the above binary interaction model to several types of blends containing copolymers and applied the model to interpret the effect of the copolymer composition in the miscibility of blends. Nevertheless, the effect of the copolymer microstructure is not always explained in terms of neighboring repulsions. In the case of poly(vinyl acetate-*co*-vinyl alcohol) (ACA) [15] or poly(vinylphenol-*co*-methyl methacrylate) (PVPh-*co*-PMMA) [16], the specific interaction between carbonyl groups and hydroxyl groups competes with hydroxyl–hydroxyl self-association. Therefore, the monomer sequential distribution in these copolymers must play an important role in determining resulting hydrogen bond distribution. The possibility of hydrogen bond formation between hydroxyl groups and neighboring carbonyl groups in the copolymer contributes to a short scale competition of specific interactions. In addition,

* Corresponding author. Tel./fax: 886 3 5131512.
E-mail address: kuosw@mail.nctu.edu.tw (S.-W. Kuo).

0032-3861/$ - see front matter © 2006 Published by Elsevier Ltd.
doi:10.1016/j.polymer.2006.03.071

the sequential distribution of the copolymer in a copolymer/homopolymer blend will also affect the charge distribution and the probability of contact between interaction sites, and consequently affect the miscibility of the blend [17].

In addition, in the ternary polymer blend, when all three binary pairs (B–A, B–C, and A–C) are individually miscible, a completely homogeneous or a closed immiscibility loop phase diagram has been observed [18]. The phase separation is caused by the difference in the interaction energy of the binary system, the so-called '$\Delta\chi$' effect and 'ΔK' effect in ternary polymer blends such as phenoxy/PMMA/PEO [19], poly(vinylphenol) (PVPh)/poly(vinyl acetate) (PVAc)/PEO [20], and poly(styrene-*co*-acrylic acid)/PMMA/PEO [21]. According to previous literature [5,16,22–24], binary pairs of PVPh/PMMA and PVPh/PEO are totally miscible over the entire compositions in the amorphous phase due to the formation of the interassociation hydrogen bonding between the hydroxyl group of PVPh and the carbonyl group of PMMA and the ether group of PEO, respectively. PEO is a highly crystalline polymer that is miscible with several weakly interacting polymers, such as PMMA [25–28], PVAc [29], and poly(vinyl pyrrolidone) [30]. Miscible blends of PEO with PMMA have been well investigated in the literature, and the results indicate that the blend components are miscible in the melt and in the amorphous phase. PEO can act as a Lewis base since the oxygen atom bears a partial negative charge, while the carbonyl carbon atom of PMMA possesses a partially positive charge. In this study, we intend to investigate the effect of different sequential distribution of a copolymer on the miscibility in copolymer/homopolymer blend by FTIR and DSC analyses. In addition, the ΔK effect was found to play a key role resulting in different phase behaviors.

2. Experimental section

2.1. Materials

The poly(vinylphenol-*co*-methyl methacrylate) (PVPh-*co*-PMMA) copolymers studied in this work were prepared by different synthetic routes as described elsewhere [16]. The block copolymer of PVPh-*b*-PMMA and random copolymer of PVPh-*r*-PMMA were synthesized by anionic and free radical copolymerization of 4-*tert*-butoxystyrene and methyl methacrylate, respectively. The *tert*-butoxy protective group was selectively removed through hydrolysis reaction. Table 1 shows the sequential distributions and molecular weights of several PVPh-*co*-PMMA copolymers employed in this study. Poly(ethylene oxide) (PEO) with $M_n = 20{,}000$ g/mol was obtained from Aldrich Co.

2.2. Blend preparation

Blends of various (PVPh-*co*-PMMA)/PEO compositions were prepared by solution casting. Tetrahydrofuran (THF) solution containing 5 wt% polymer mixtures was stirred for 6–8 h and then cast onto a Teflon dish and was left to evaporate slowly at room temperature for 1 day. The blend film was then dried at 50 °C for 2 days.

2.3. Measurements

All infrared spectra were recorded at 25 °C at a resolution of 1 cm^{-1} on a Nicolet AVATAR 320 FTIR spectrometer. Each sample was dissolved in THF and then cast directly onto KBr pellets. All films were vacuum-dried and were thin enough to be within the absorbance range where the Beer–Lambert law is obeyed. Because these samples containing hydroxyl groups are water sensitive, a pure nitrogen flow was used to purge the IR optical box in order to maintain sample film dryness. All infrared spectra in carbonyl region use the normalize intensity, which compared with the free carbonyl group of pure PMMA. Thermal analysis was performed on a DSC instrument from Du-Pont (DSC-9000) at a scan rate of 20 °C/min over a temperature ranging from 20 to 250 °C. The sample was quenched to −120 °C from the melt state for the first scan and then rescanned between −120 and 250 °C at 20 °C/min. The glass transition temperature was obtained at the inflection point of the heat capacity jump.

3. Results and discussion

3.1. Thermal analyses

The PVPh is totally miscible with PEO and PMMA in the amorphous phase due to the formation of the interassociation hydrogen bonding between the hydroxyl group of the PVPh and the carbonyl group of the PMMA and the ether group of the PEO, respectively, [22–24]. In addition, PEO and PMMA are also fully miscible in the amorphous phase [25–28]. In general, differential scanning calorimetry (DSC) is one of the convenient methods to determine the miscibility in polymer blends. Fig. 1 shows the conventional second run DSC thermograms of PVPh-*r*-PMMA/PEO blends of various compositions; it reveals that each blend composition has a single glass transition temperature. A single value of T_g strongly suggests that the PVPh-*r*-PMMA/PEO blend system is fully miscible in the homogeneous amorphous phase. Table 2 summarizes the thermal properties of PVPh-*r*-PMMA, PEO, and their blends. At higher PEO contents, PEO crystallizes

Table 1
Characterization of PVPh-*r*-PMMA prepared by free radical polymerization and PVPh-*b*-PMMA synthesized by anionic polymerization

PVPh-*r*-PMMA	M_n (g/mol)	Composition of PVPh (wt%)	M_w/M_n	PVPh-*b*-PMMA	M_n (g/mol)	Composition of PVPh (wt%)	M_w/M_n
30-*r*-70	18,000	30	1.62	30-*b*-70	16,000	30	1.11
58-*r*-42	19,000	58	1.63	40-*b*-60	16,000	40	1.15
76-*r*-24	17,600	76	1.49	55-*b*-45	30,000	55	1.10
92-*r*-8	16,000	92	1.63	75-*b*-25	22,000	75	1.13

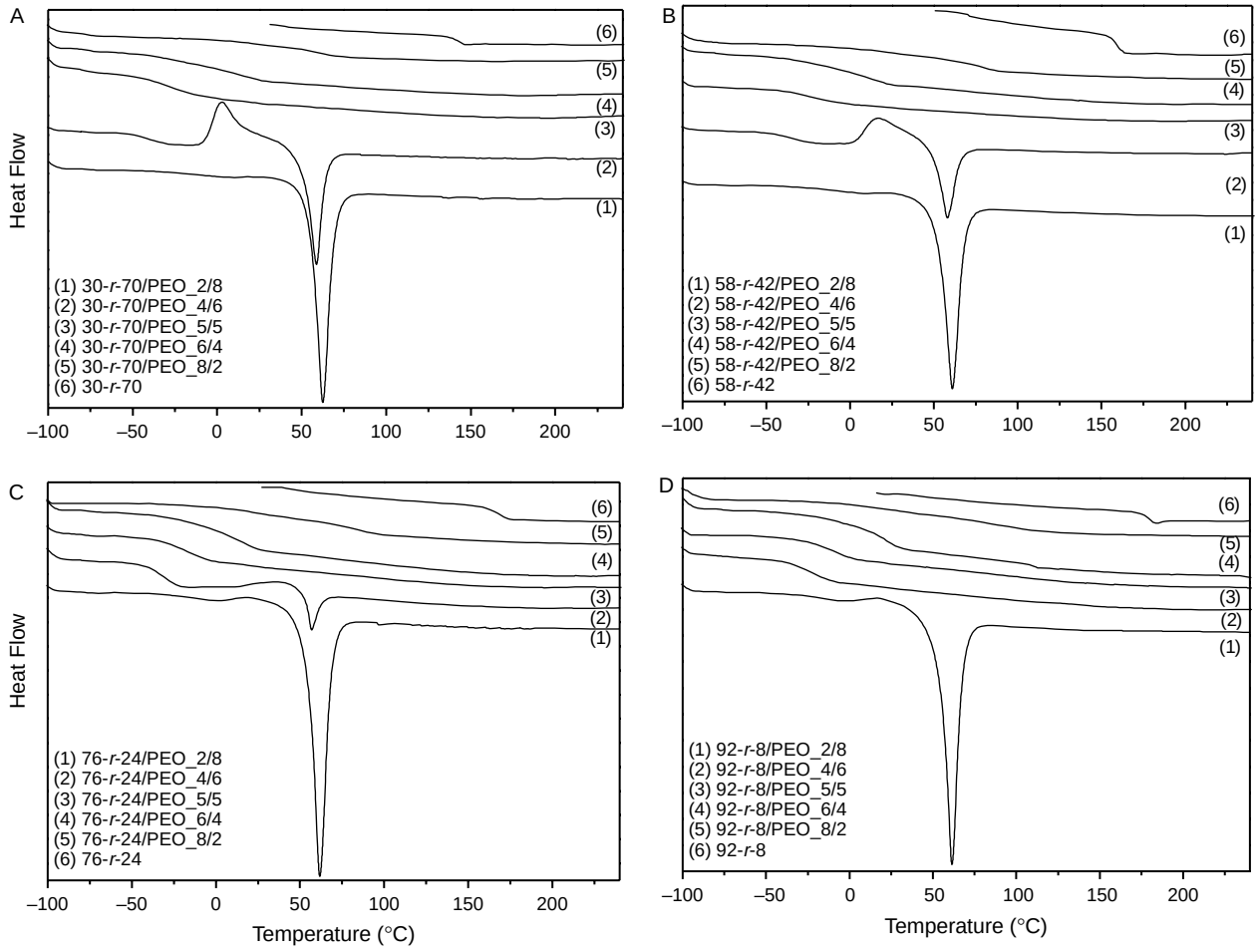

Fig. 1. DSC thermograms of PVPh-*r*-PMMA/PEO blends having different compositions for (A) 92-*r*-8/PEO, (B) 76-*r*-24/PEO, (C) 58-*r*-42/PEO, and (D) 30-*r*-70/PEO.

from the molten mixture of PEO and PVPh-*r*-PMMA copolymer. The melting temperature of the PEO component decreases with increasing the PVPh-*r*-PMMA copolymer content in the blend. The melting temperature also decreases with increasing the PVPh content in the PVPh-*r*-PMMA copolymer at the same blend ratio. This phenomenon suggests that the PVPh-*r*-PMMA copolymer in the blend hinders the crystallization of PEO, which is a typical phenomenon of a miscible blend in which the glass transition temperature of an amorphous polymer is higher than that of a crystalline component. Furthermore, the dependence of T_g on the composition of the miscible PVPh-*r*-PMMA/PEO blends is shown in Fig. 2(A). Clearly, the values of T_g of each PVPh-*r*-PMMA/PEO blend shift to lower temperatures as the PEO content increases in the blend. However, the upturn of the values of T_g at higher PEO content is due to the crystallization of PEO during quenching. This phenomenon suggests that not only the crystallization of PEO in the blends can change the amorphous phase but also the crystal of PEO is able to act as a physical cross-linking point that may hinder the molecular mobility of amorphous phase [31,32].

Fig. 3 displays the second run DSC thermograms of PVPh-*b*-PMMA/PEO blends. Again, the binary PVPh/PMMA, PVPh/PEO, and PMMA/PEO blends are all fully miscible in the amorphous phase. However, the DSC thermograms of 30-*b*-70/PEO = 8/2, 7/3, and 40-*b*-60/PEO = 8/2 show two T_gs (see insertion figures), implying that they are phase-separated in the amorphous phase. The thermal properties of PVPh-*b*-PMMA/PEO blends were summarized in Table 3 and the dependence of T_g on the composition of the miscible PVPh-*b*-PMMA/PEO blends is shown in Fig. 2(B). Clearly, the thermal behavior of PVPh-*b*-PMMA/PEO blends has the similar tendency to the PVPh-*r*-PMMA/PEO blends, which suggests a molecular approach to the similarities.

3.2. FT-IR analyses

Infrared spectroscopy has been used to detect the existence of specific interactions in polymer blends. This tool can be used to study the mechanism of interpolymer miscibility through the bond formation both qualitatively and quantitatively. Several regions within the infrared spectra of PVPh-*co*-PMMA/PEO blends are influenced by the hydrogen-bonding interaction.

Fig. 4(A) shows infrared spectra in the 3050–3750 cm^{-1} range for the pure PVPh. This broad band can be considered to be composed of narrow contributions corresponding to hydroxyl groups surrounded by different environments: hydroxyl groups

Table 2
Thermal properties of PVPh-*r*-PMMA/PEO blends

Copolymer	PEO content (wt%)	T_g (°C)	T_m (°C)
30-*r*-70	0	143	
	20	58	
	40	0	
	50	−32	
	60	−39	58.7
	80	−6	62.5
	100	−67	69.2
58-*r*-42	0	160	
	20	78	
	40	11	
	50	−18	
	60	−35	58.1
	80	−11	61.8
76-*r*-24	0	169	
	20	81	
	40	14	
	50	−18	
	60	−32	56.9
	80	−17	61.4
92-*r*-8	0	179	
	20	87	
	40	21	
	50	−9	
	60	−20	
	80	−17	61.0

hydrogen bonded with other hydroxyl groups in the same or vicinal chains (forming dimmers, trimers, etc.), and non-hydrogen bonded hydroxyl groups [33]. In addition, the spectra of the miscible 92-*r*-8/PEO blends show significant changes in this region, suggesting a redistribution of electron density in the arrangement of the hydroxyl group association. These data indicate that there are many different types of hydroxyl groups present in PVPh-*r*-PMMA copolymers and PVPh-*r*-PMMA/PEO blends. In the meantime, the spectrum of pure PVPh shown in Fig. 4(A) is characterized by a very broad band centered at 3350 cm^{-1}, indicating that these hydroxyl groups are hydrogen bonded to other hydroxyl groups as dimmers and chain-like multimers. A second narrower band, observed at 3525 cm^{-1} as a shoulder on the high frequency side of the broad hydrogen bonded band, is assigned to free hydroxyl groups [5]. Taking into account the effect of composition, the hydrogen bonding between carbonyl groups of methyl methacrylate and the hydroxyl group of vinyl phenol competes with self-associated hydroxyl groups for hydrogen bonding and cause the shift of the hydroxyl band toward higher wavenumbers at lower vinylphenol content. In this situation, majority of only one type of hydroxyl group from the hydrogen-carbonyl inter-association is expected, and thus the hydroxyl stretching band is relatively narrower. On the contrary, the free, dimer, or multimer hydrogen bonded hydroxyl groups will exist at higher vinylphenol contents, which resulting in broader absorptions. Therefore, the spectrum of 30-*r*-70 copolymer shown in Fig. 4(B) is reasonable to assign the band at 3440 cm^{-1} to the hydroxyl groups interacting with carbonyl groups because the small numbers of the hydroxyl groups tend to interact completely with carbonyl groups. When comparing the spectra corresponding to the same system as a function of composition, a progressive shift of this band toward lower wavenumber is observed for increasing content of ether oxygen of PEO (Fig. 4). This behavior suggests that a significant part of the hydroxyl groups involved in the association processes previously described for PVPh-*r*-PMMA copolymer are now hydrogen bonded to ether oxygen groups in PEO.

In the case of PVPh-*b*-PMMA/PEO blends (Fig. 5), infrared spectra show a clear shift of the hydroxyl band toward lower wavenumbers, relative to that of the pure PVPh-*b*-PMMA copolymer. As the PEO content in the blend increases, the band gradually shift to lower frequencies, providing additional evidence for the existence of hydrogen bonding interaction between the PEO ether group and the hydroxyl group of PVPh.

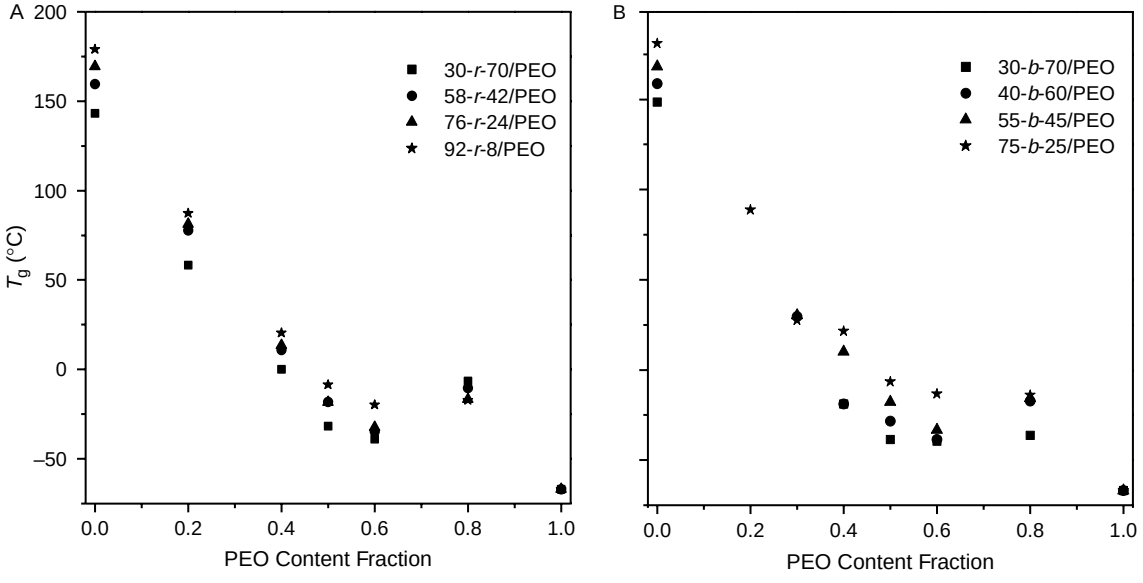

Fig. 2. Plots of T_g vs. weight of PEO for the copolymer/PEO (A) PVPh-*r*-PMMA/PEO and (B) PVPh-*b*-PMMA/PEO blends.

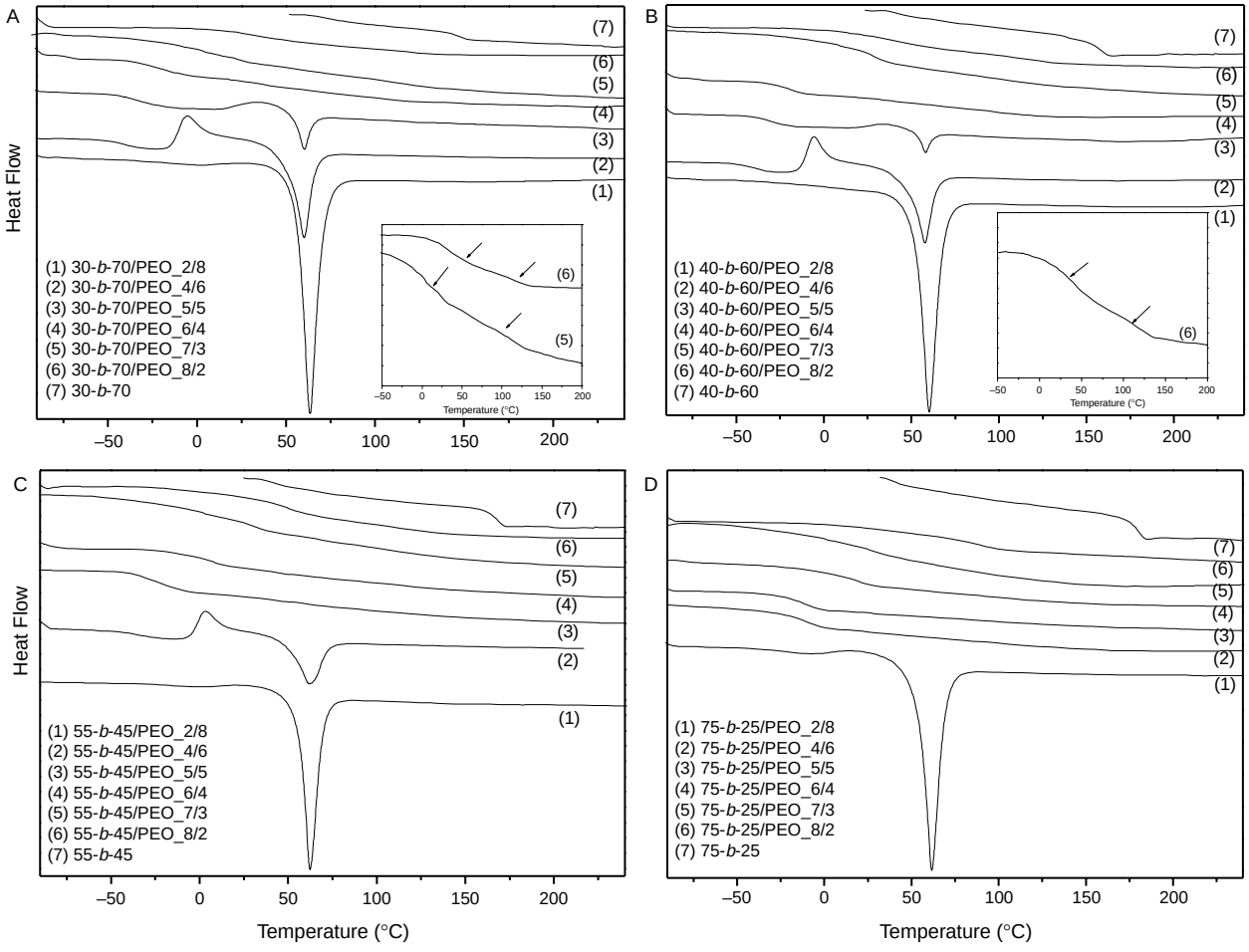

Fig. 3. DSC thermograms of PVPh-*b*-PMMA/PEO blends having different compositions for (A) 75-*b*-25/PEO, (B) 55-*b*-45/PEO, (C) 40-*b*-60/PEO, and (D) 30-*b*-70/PEO.

The frequency difference between the free hydroxyl absorbance and the hydrogen bonded hydroxyl ($\Delta\nu$) is a measure of the average strength of the intermolecular interactions [34,35]. For instance, we use the position of the free hydroxyl stretching vibration at 3525 cm^{-1} as a reference, then the median frequency difference for hydroxyl–hydroxyl self-association in PVPh is about 175 cm^{-1} while that of the interassociation between hydroxyl groups of PVPh and carbonyl groups of PMMA is 85 cm^{-1}. Fig. 6 displays the frequency difference ($\Delta\nu$) in FTIR of all PVPh-*r*-PMMA/PEO and PVPh-*b*-PMMA/PEO blends at room temperature vs. PEO content. The $\Delta\nu$ of PVPh-*r*-PMMA/PEO and PVPh-*b*-PMMA/PEO blend system exhibits the same increasing trend as the PEO content is increased. In the 30-*r*-70/PEO = 4/6 blend, there is no evidence of free hydroxyl and the concentration of hydroxyl–hydroxyl interactions appears insignificant. Therefore, it is reasonable to assign the band at 3150 cm^{-1} to the hydroxyl groups of PVPh hydrogen bonded to ether oxygens of the PEO in the PVPh-*r*-PMMA/PEO system. The frequency difference between the free hydroxyl band and the band attributed to hydroxyl groups hydrogen bonded to ether oxygens is about 375 cm^{-1}. This is somewhat greater than that observed for PVPh-*b*-PMMA/PEO system (ca. 350 cm^{-1}) and presumably reflects a moderate increase in the relative strength of the PVPh-*r*-PMMA/PEO intermolecular interaction; a reasonable conclusion considering the enhanced affinity for hydrogen bonding of the hydroxyl groups in PVPh-*r*-PMMA compared to that in PVPh-*b*-PMMA. However, these values of $\Delta\nu$ in all copolymer/PEO blends also imply that the interassociation between PVPh and PEO is considerably stronger than either the self-association of hydroxyl groups in PVPh or the interactions between hydroxyl groups in PVPh and carbonyl groups in PMMA.

The CH_2 wagging region of the pure PEO and its blends with PVPh-*co*-PMMA copolymer is now examined. Figs. 7 and 8 show infrared spectra in the 1320–1380 cm^{-1} region of the pure PEO, and various PVPh-*co*-PMMA/PEO blends at room temperature. The pure PEO has two bands at 1360 and 1343 cm^{-1} that represent the crystalline phase of the PEO [36]. These bands decrease as the PVPh-*co*-PMMA content is increased. These crystalline bands disappear on PVPh-*r*-PMMA/PEO = 4/6 and PVPh-*b*-PMMA/PEO = 5/5 blends and are replaced by a broad band roughly centered at 1350 cm^{-1} corresponding to the amorphous phase. That means the PEO crystallization is being retarded or even inhibited by adding the amorphous PVPh-*co*-PMMA copolymer. As a result, we can confirm that the hydroxyl group of PVPh is more

Table 3
Thermal properties of PVPh-*b*-PMMA/PEO blends

Copolymer	PEO content (wt%)	T_g (°C)	T_m (°C)
30-*b*-70	0	149	
	20	28, 116	
	30	3, 119	
	40	−19	
	50	−39	60.3
	60	−40	60.2
	80	−36	63.5
	100	−67	69.2
40-*b*-60	0	159	
	20	37, 111	
	30	30	
	40	−19	
	50	−28	58.1
	60	−39	57.8
	80	−1	60.2
55-*b*-45	0	168	
	20	51, 111	
	30	30	
	40	10	
	50	−18	
	60	−33	62.0
	80	−16	62.3
75-*b*-25	0	181	
	20	89	
	30	28	
	40	22	
	50	−7	
	60	−8	
	80	−14	61.6

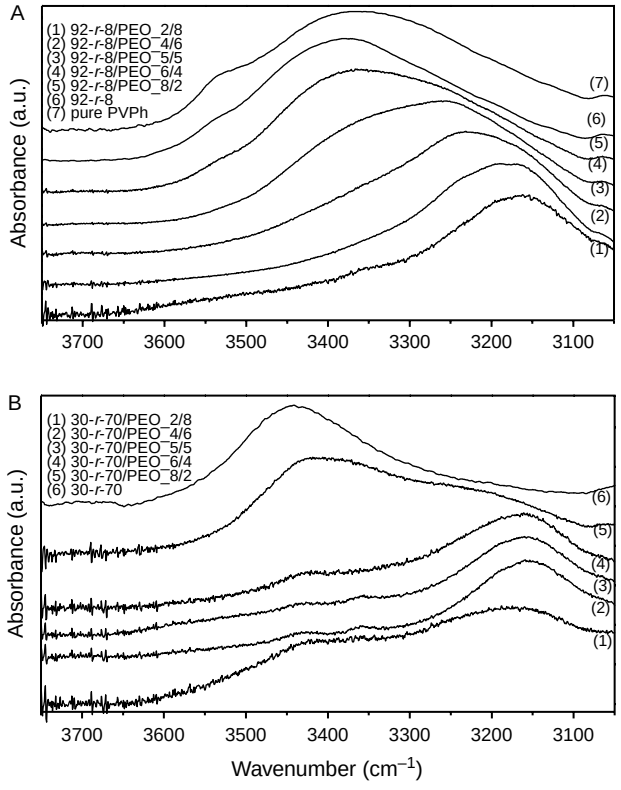

Fig. 4. FTIR spectra in the 3050–3750 cm^{-1} region for (A) 92-*r*-8/PEO and (B) 30-*r*-70/PEO.

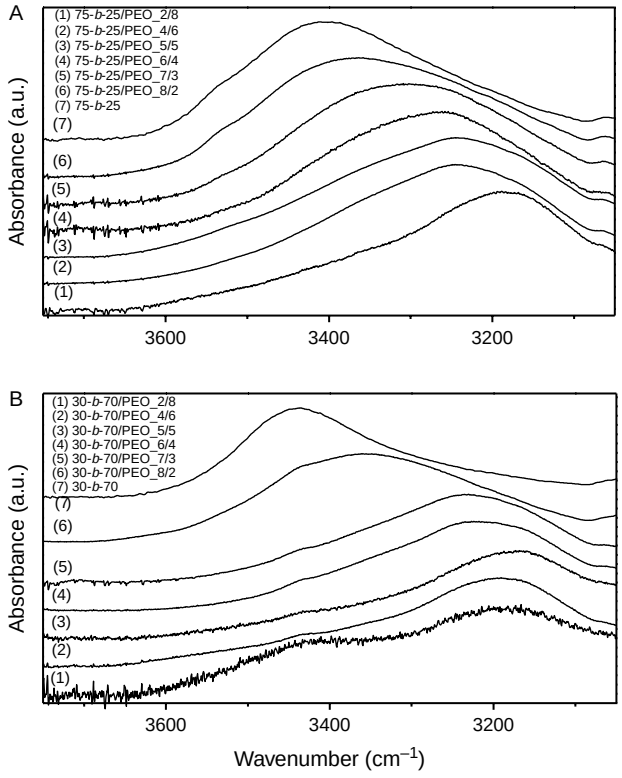

Fig. 5. FTIR spectra in the 3050–3750 cm^{-1} region for (A) 75-*b*-25/PEO and (B) 30-*b*-70/PEO.

favorable to form the interassociation with ether group of PEO than with carbonyl group of PMMA. However, the difference in crystallization behaviors was investigated by DSC and FTIR on 30-*r*-70/PEO = 4/6 and 30-*b*-70/PEO = 5/5 blends. In general, the polymer crystallinity measured by FTIR is from direct sample measurement, and no thermal history is involved in preparing the sample. On the contrary, the polymer crystallinity detected by DSC depends on the thermal history because recrystallization may occur during cooling or heating scan.

We now turn our attention to Fig. 6 again. The frequency difference ($\Delta\nu$) increases with increasing PEO content and approaches a maximum for the blend containing 60 wt% PEO except the 92-*r*-8/PEO and 75-*b*-25/PEO blends, in which they show $\Delta\nu$ decrease with further increase of the PEO content. The observed slight decrease in $\Delta\nu$ at higher PEO content (80 wt%) can be explained by the fact that these blend systems possess PEO crystalline phase. Consequently, the hydroxyl–ether interassociation tends to decrease between the PVPh and PEO segments due to reduced chain mobility in the PEO crystalline phase [37]. In another aspect, since more hydroxyl groups are present at the interface between PVPh-*co*-PMMA copolymer and PEO crystalline phase in the 92-*r*-8/PEO = 2/8 and 75-*b*-25/PEO = 2/8 blends, the hydroxyl stretching bands do not shift back to higher wavenumber.

The carbonyl stretching band for PMMA appears at 1730 cm^{-1}. Figs. 9 and 10 show the infrared spectra of the carbonyl stretching measured at room temperature ranging from 1670 to 1770 cm^{-1} of PVPh-*co*-PMMA and PVPh-*co*-PMMA/PEO blends. The carbonyl stretching of the pure

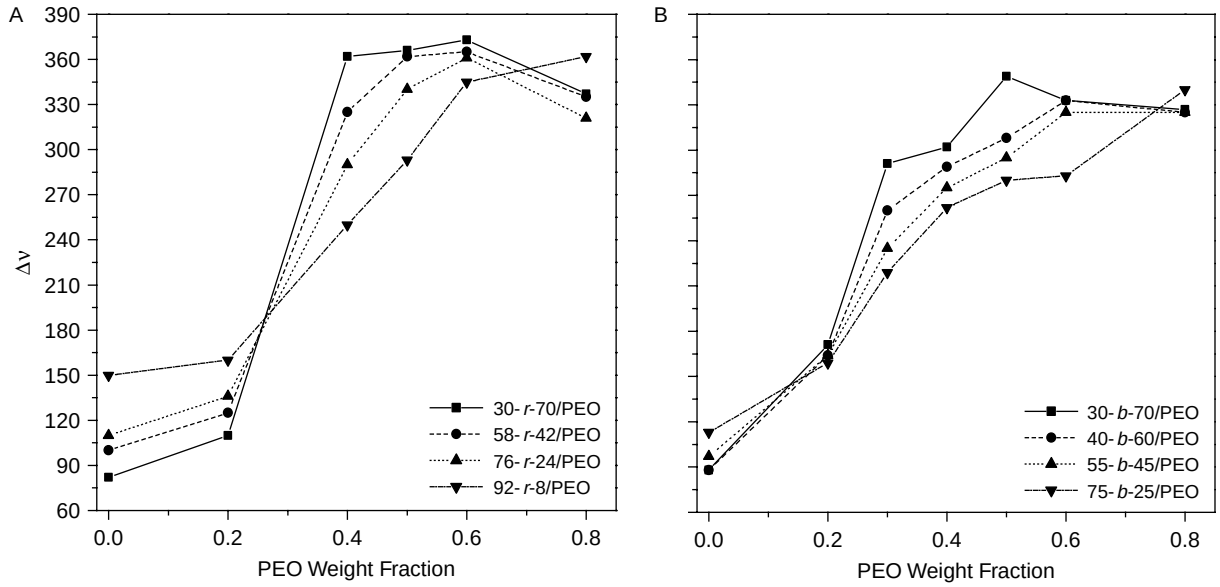

Fig. 6. Plots of $\Delta\nu$ vs. weight of PEO for the copolymer/PEO (A) PVPh-*r*-PMMA/PEO and (B) PVPh-*b*-PMMA/PEO blends.

PVPh-*co*-PMMA is split into two bands, absorption by free and hydrogen bonded carbonyl groups at 1730 and 1705 cm^{-1}, respectively. Obviously, the relative contribution of these two types of carbonyl groups must be dependent on copolymer composition. As has been observed in infrared spectra, we can expect a higher fraction of hydrogen bonded carbonyl groups for copolymers rich in vinyl phenol units where carbonyl groups are more surrounded by the donor medium. As can be seen in Figs. 9 and 10, the presence of ether groups in these blend leads to a competition with carbonyl groups for hydrogen bonding with hydroxyl groups. This competition is evident in the evolution of the carbonyl band in the blend. Thus, for a particular PVPh-*co*-PMMA copolymer, the hydrogen bonded carbonyl groups (progressive decrease of the shoulder at relatively lower wavenumber) decrease with the increase of the PEO content in the blend increases. In other word, the hydroxyl–ether association prevails over the hydroxyl–carbonyl association. This result is in

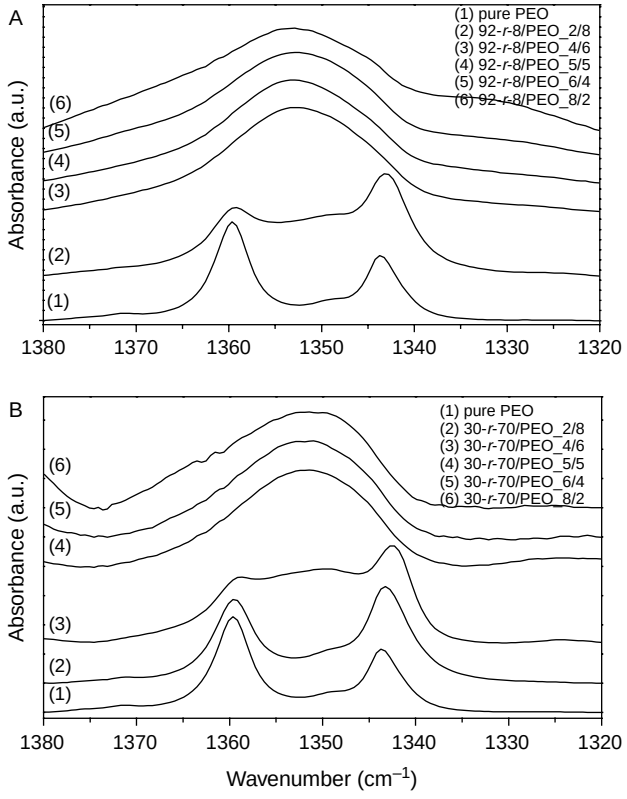

Fig. 7. FTIR spectra in the 1320–1380 cm^{-1} region for (A) 92-*r*-8/PEO and (B) 30-*r*-70/PEO.

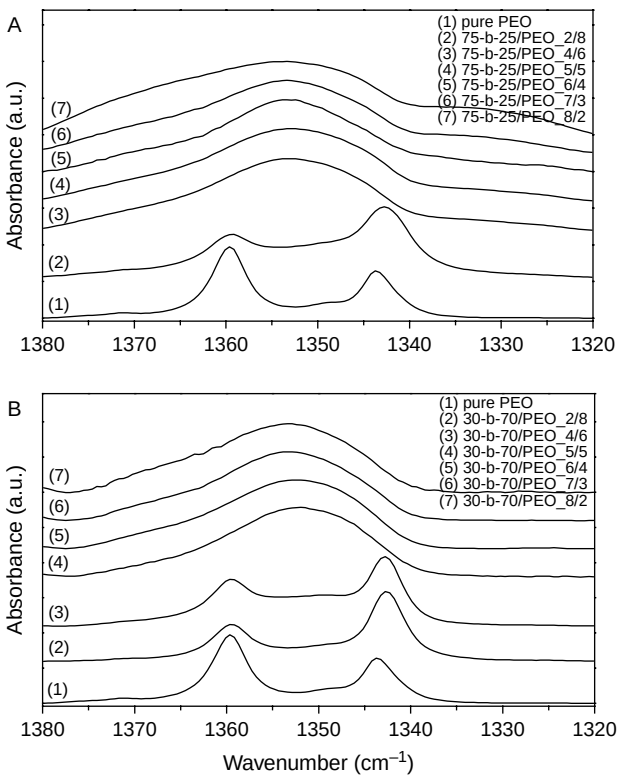

Fig. 8. FTIR spectra in the 1320–1380 cm^{-1} region for (A) 75-*b*-25/PEO and (B) 30-*b*-70/PEO.

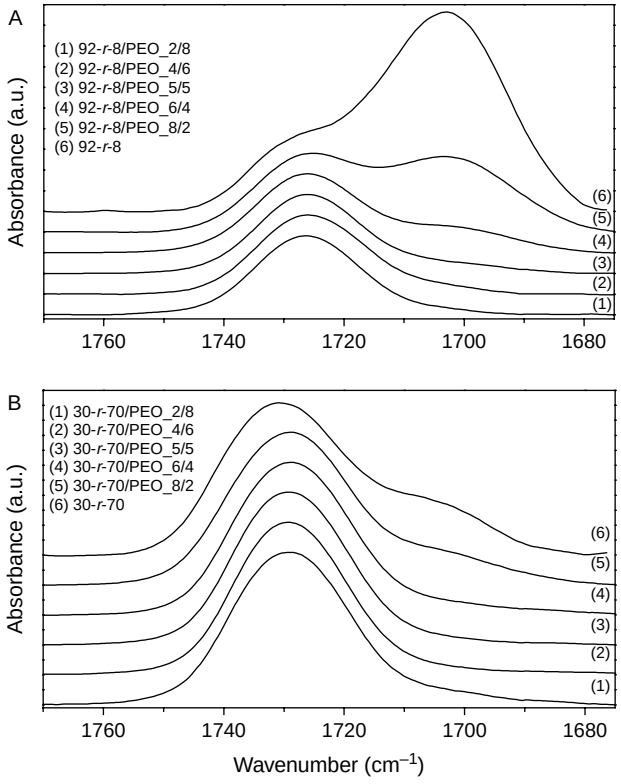

Fig. 9. FTIR spectra (1670–1780 cm^{-1}) of a (A) 92-*r*-8/PEO and (B) 30-*r*-70/PEO.

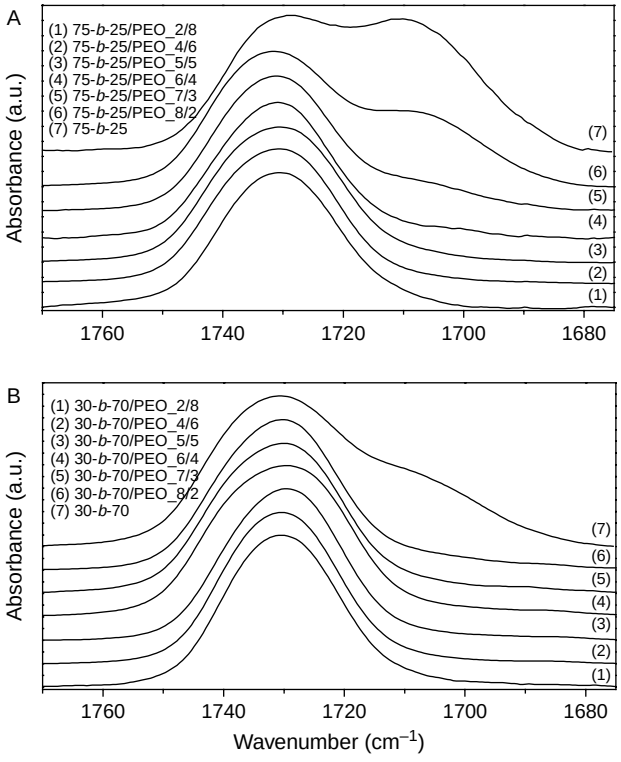

Fig. 10. FTIR spectra (1670–1780 cm^{-1}) of a (A) 75-*b*-25/PEO and (B) 30-*b*-70/PEO.

agreement with the evolution previously reported for the hydroxyl stretching region.

These bands can be readily decomposed into two Gaussian peaks, the free carbonyl (1730 cm^{-1}) and the hydrogen bonded carbonyl (1705 cm^{-1}) absorptions. Using the known respective absorptivity coefficients, fractions of these two types of carbonyl groups can be calculated from the relative intensities of these two bands. To obtain the fraction of the hydrogen bonded carbonyl group, a known absorptivity ratio for hydrogen bonded and free carbonyl is required. We employed a value of $\alpha_{HB}/\alpha_F = 1.5$, which was previously calculated by Moskala et al. [38]. Tables 4 and 5 summarize fractions of hydrogen-bonded carbonyl calculated through curve fitting of the data from both copolymers and their blends. Tables 4 and 5 show that the fraction of hydrogen bonded carbonyl decreases with increasing the relative ratio of PEO to PMMA. This result implies that the interassociation equilibrium constant of hydroxyl–ether is greater than the interassociation equilibrium constant of hydroxyl–carbonyl and the self-association equilibrium constant of hydroxyl–hydroxyl at room temperature. In our previous study [37,39], we have used three competing functional groups to predict the fraction of hydrogen bonded carbonyl group. According to the Painter–Coleman Association Model (PCAM), we designate B, A, and C as PVPh, PMMA, and PEO, respectively. K_2, K_B, K_A, and K_C are their respective association equilibrium constants.

$$B_1 + B_1 \overset{K_2}{\leftrightarrow} B_2 \tag{1}$$

$$B_h + B_1 \overset{K_B}{\leftrightarrow} B_{h+1} (h \geq 2) \tag{2}$$

$$B_h + C_1 \overset{K_C}{\leftrightarrow} B_h C \tag{3}$$

$$B_h + A_1 \overset{K_A}{\leftrightarrow} B_h A \tag{4}$$

These four equilibrium constants can be expressed as follows in terms of volume fractions

$$\Phi_B = \Phi_{B1} \Gamma_2 \left[1 + \frac{K_A \Phi_{A1}}{r_A} + \frac{K_C \Phi_{C1}}{r_C} \right] \tag{5}$$

$$\Phi_A = \Phi_{A1} [1 + K_A \Phi_{B1} \Gamma_1] \tag{6}$$

$$\Phi_C = \Phi_{C1} \left[1 + K_C \Phi_{B1} \Gamma_1 \right] \tag{7}$$

where

$$\Gamma_1 = \left(1 - \frac{K_2}{K_B} \right) + \frac{K_2}{K_B} \left(\frac{1}{1 - K_B \Phi_{B1}} \right) \tag{8}$$

$$\Gamma_2 = \left(1 - \frac{K_2}{K_B} \right) + \frac{K_2}{K_B} \left(\frac{1}{(1 - K_B \Phi_{B1})^2} \right) \tag{9}$$

Φ_B, Φ_A, and Φ_C are the volume fractions of repeat units in the blend, Φ_{B1}, Φ_{A1}, and Φ_{C1} are the volume fractions of isolated units in the blend, and $r_A = V_A/V_B$ and $r_C = V_C/V_B$ are the ratios of segmental molar volumes.

Table 4
Results of curve-fitting the data for PVPh-*r*-PMMA/PEO blends at room temperature

PVPh-*random*-PMMA/PEO	H-bonded C=O			Free C=O			f_b[a]
	ν (cm^{-1})	$W_{1/2}$ (cm^{-1})	A_b (%)	ν (cm^{-1})	$W_{1/2}$ (cm^{-1})	A_f (%)	
92-*r*-8	1703	24	82.3	1729	18	17.7	75.7
92-*r*-8/PEO_8/2	1703	24	55.7	1727	19	44.3	45.6
92-*r*-8/PEO_6/4	1704	24	29.5	1726	19	70.5	21.8
92-*r*-8/PEO_5/5	1705	24	16.1	1726	19	83.9	11.3
92-*r*-8/PEO_4/6	1706	24	10.9	1726	19	88.1	7.6
92-*r*-8/PEO_2/8	1705	24	5.5	1726	19	94.5	3.7
76-*r*-24	1704	25	75.7	1729	19	24.3	65.6
76-*r*-24/PEO_8/2	1704	24	43.5	1728	18	56.2	34.0
76-*r*-24/PEO_6/4	1704	24	19.4	1727	18	80.9	13.7
76-*r*-24/PEO_5/5	1703	24	11.2	1727	18	89.0	7.7
58-*r*-42	1704	25	59.6	1730	19	40.4	49.3
58-*r*-42/PEO_8/2	1704	24	35.1	1729	19	64.9	26.5
58-*r*-42/PEO_6/4	1703	23	16.5	1728	19	83.5	11.6
30-*r*-70	1706	24	35.6	1730	19	64.4	26.9
30-*r*-70/PEO_8/2	1705	23	16.8	1730	19	83.2	11.8

[a] f_b: fraction of hydrogen bonded carbonyl group.

The self-association constant of PVPh (hydroxyl–hydroxyl), the interassociation constant between PMMA and PVPh (carbonyl–hydroxyl), and the interassociation constant between PEO and PVPh (ether–hydroxyl) in PVPh-*r*-PMMA/-PEO blend have been reported in the literature [16,40,41]. The interassociation constant of PEO in PVPh-*b*-PMMA/PEO blend is determined indirectly from a least-squares fitting procedure. If these equilibrium constants (K_2, K_B, K_A), segment molar volume, and the fraction of hydrogen bonded carbonyl group are known, the K_C value can be calculated from Eqs. (5)–(9) by using a least-squares fitting based on the fraction of hydrogen bonded carbonyl group experimentally obtained. We obtained the value for $K_C = 300$ in PVPh-*b*-PMMA/PEO blend system at room temperature, implying that the interassociation equilibrium constant for hydroxyl–ether is indeed greater than the interassociation equilibrium constant of hydroxyl–carbonyl and self-association equilibrium constant of PVPh at room temperature. Table 6 lists all the parameters required by the Painter–Coleman association model to estimate thermodynamic properties for these PVPh-*co*-PMMA/PEO blends. These results give a good agreement between the experimental and theoretical fractions of the hydrogen bonded carbonyl groups corresponding based on PVPh-*r*-PMMA/PEO and PVPh-*b*-PMMA/PEO blends by using a fixed volume fractions of PEO ($\Phi_C = 0.2$) as illustrated in Fig. 11. The observed difference in K_C values between these two PVPh-*co*-PMMA/PEO blends can be attributed to the 'screening' or locally nonrandom mixing driven primarily by intramolecular connectivity effects [41,42]. The covalent linkages within polymer segments of a copolymer result in greater numbers of same-chain contacts than that calculated from a random mixing of segments.

The interassociation equilibrium constant of PEO ($K_C = 231$ obtained from PVPh-*r*-PMMA/PEO blends and $K_C = 300$ obtained from PVPh-*b*-PMMA/PEO blends) is greater than the interassociation equilibrium constant (hydroxyl–carbonyl) of PVPh-*r*-PMMA ($K_A = 67.4$) or PVPh-*b*-PMMA ($K_A = 47.1$). When PEO is mixed with PVPh-*co*-PMMA, its ether oxygen competes for the PVPh hydroxyl and f_b of PMMA in both copolymer/PEO blends inevitably decreases. Meanwhile, the

Table 5
Results of curve-fitting the data for PVPh-*b*-PMMA/PEO blends at room temperature

PVPh-*block*-PMMA/PEO	H-bonded C=O			Free C=O			f_b
	ν (cm^{-1})	$W_{1/2}$ (cm^{-1})	A_b (%)	ν (cm^{-1})	$W_{1/2}$ (cm^{-1})	A_f (%)	
75-*b*-25	1709	25	65.8	1732	18	34.2	56.2
75-*b*-25/PEO_8/2	1708	24	35.3	1732	18	64.7	26.6
75-*b*-25/PEO_7/3	1707	24	17.6	1731	18	82.4	12.4
75-*b*-25/PEO_6/4	1707	23	5.3	1731	18	94.7	3.6
55-*b*-45	1708	24	58.3	1733	19	41.7	48.2
55-*b*-45/PEO_8/2	1707	23	24.8	1731	19	75.2	18.0
55-*b*-45/PEO_7/3	1706	23	8.6	1731	19	91.4	6.0
40-*b*-60	1709	24	42.1	1732	19	57.9	32.6
40-*b*-60/PEO_8/2	1707	23	14.9	1731	19	85.1	10.4
40-*b*-60/PEO_7/3	1707	23	7.2	1731	19	92.8	4.8
30-*b*-70	1709	23	32.8	1732	20	67.2	24.6
30-*b*-70/PEO_8/2	1707	23	11.5	1731	19	88.5	7.7

Table 6
Summary of the self-association and interassociation parameters of PVPh-*co*-PMMA copolymers and PVPh-*co*-PMMA/PEO blends

Polymer	Molar volume (ml/mol)	Molecular weight (g/mol)	Solubility parameter $(cal/ml)^{0.5}$	Self-association equilibrium constant		Interassociation equilibrium constant					
						Random copolymer		Block copolymer		Ternary polymer blend	
				K_2	K_B	K_A	K_C	K_A	K_C	K_A	K_C
PVPh	100.0	120.0	10.6	21.0	66.8						
PMMA	84.9	100.0	9.1			67.4[a]		47.1[b]		37.4[a]	
PEO	38.1	44.1	9.4				231[c]		300[d]		490[e]

[a] Ref. [40].
[b] Ref. [16].
[c] Ref. [41].
[d] This work.
[e] Ref. [20].

fraction of hydrogen bonded carbonyl of PVPh-*r*-PMMA/PEO blend is greater than that of PVPh-*b*-PMMA/PEO blend under the similar composition based on higher K_A (67.4 vs. 47.1). The f_b listed in Tables 4 and 5 indeed show the expected trend. In another aspect, someone may speculate that the observed higher $\Delta\nu$ of PVPh-*b*-PMMA/PEO blend is greater than that of PVPh-*r*-PMMA/PEO blend due to the relative ratio of interassociation equilibrium constant of PEO to PMMA is larger in PVPh-*b*-PMMA/PEO blend system. However, we have displayed the opposed experiment results in Fig. 6. This phenomenon can be rationalized by the so-called $\Delta\chi$ effect and ΔK effect in a ternary blend.

The phase behavior of a ternary polymer blend system is primarily governed by the magnitude of the individual binary interaction parameters (χ_{ij} if no strong specific interaction is present. There is a driving force towards phase separation if the difference in the interaction parameter values is significantly high and results in a $\Delta\chi$ effect, which is unfavourable 'physical' interaction. When there is hydrogen bonding interactions present in a polymer blend, higher difference in interassociation equilibrium constant tends to induce phase separation. The ΔK effect reflects the difference in the 'chemical' interaction between the self-association polymer and the other polymers in the mixture. While the presence of specific intermolecular interactions enhances the probability of forming a homogeneous ternary polymer blend, they can concurrently exacerbate the situation through the ΔK effect, which tends to promote phase separation. By taking into account these two effects simultaneously, it is difficult to find ternary polymer blends that exist homogeneously over a wide composition range [43,44].

The phase diagrams of both PVPh-*co*-PMMA/PEO blends are shown in Fig. 12(A) and (B) based on DSC results listed in Tables 2 and 3. For comparison, the phase diagram of PVPh/PMMA/PEO ternary polymer blend is also displayed in Fig. 12(C) and their thermal properties are listed in Table 7. As can been seen, the PVPh-*r*-PMMA/PEO blend system exhibits a single phase over the entire compositions. On the other hand, there exists a closed-looped of phase separated region in the phase diagrams of PVPh-*b*-PMMA/PEO and PVPh/PMMA/PEO due to the so-called $\Delta\chi$ and ΔK effects in ternary polymer blends. The non-hydrogen bonded solubility

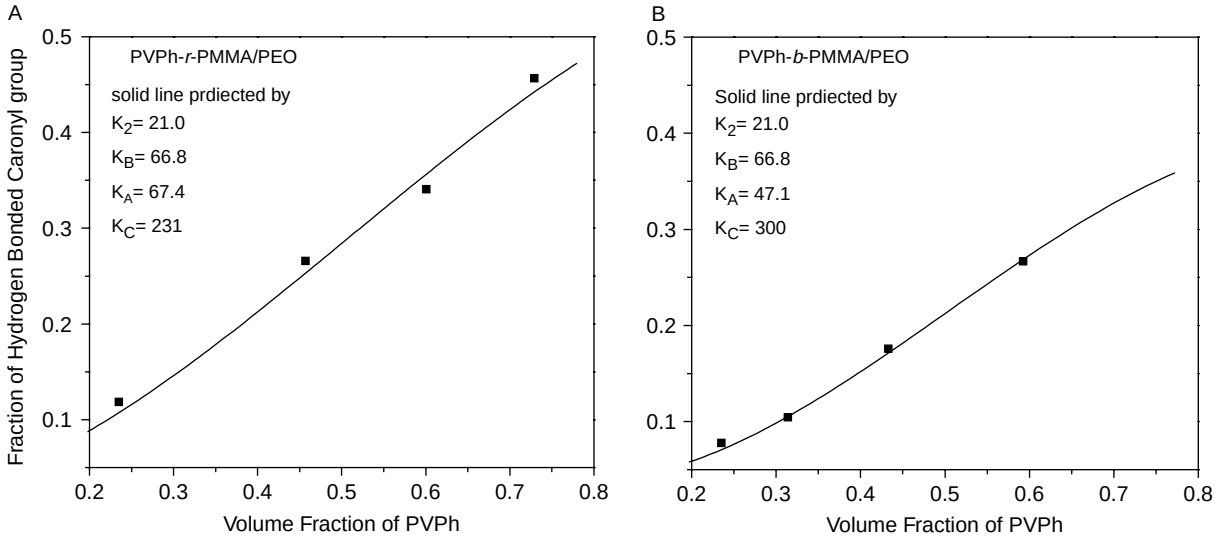

Fig. 11. Plot of the calculated (—) and experimental (■)values of the fraction of hydrogen bonded carbonyl groups in blends of (A) PVPh-*r*-PMMA/PEO and (B) PVPh-*b*-PMMA/PEO blends where the volume fraction of PEO was hold at 0.2.

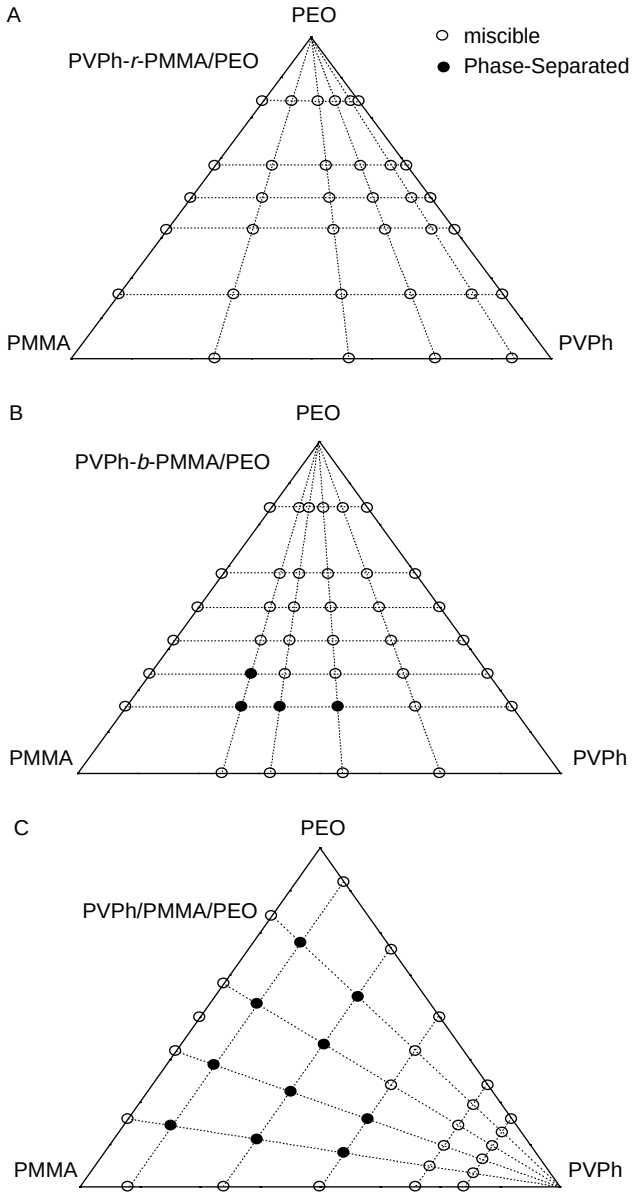

Fig. 12. Ternary phase diagram of (A) PVPh-*r*-PMMA/PEO and (B) PVPh-*b*-PMMA/PEO blends. The open circles represent a miscible ternary blend, and the full circles represent an phase-separated ternary blend.

parameters of the specific repeat units for these two PVPh-*co*-PMMA/PEO blend systems are the same, implying that the contribution to the free energy of mixing from physical force in the two blend systems is essentially identical. Furthermore, ΔK is related to the ratio of the two interassociation equilibrium constants, K_C/K_A. Consequently, the closed-loop of heterogeneous region is formed in PVPh-*b*-PMMA/PEO blend system caused by greater ΔK effect. In addition, the PVPh-*r*-PMMA/PEO blend system has greater homogeneity at the molecular scale than that of the PVPh-*b*-PMMA/PEO blend system based on DSC analyses. In addition, the strength of the hydrogen bond formed between the hydroxyl and ether in PVPh-*r*-PMMA/PEO blends is higher than that in PVPh-*b*-PMMA/PEO blends. As a result, the $\Delta\nu$ of PVPh-*r*-PMMA/PEO blend is higher than that of PVPh-*b*-PMMA/PEO blend, implying that the ΔK effect plays a more important role in dictating the ability of hydrogen bond formation and the miscibility in the ternary polymer blend.

Table 7
Thermal properties of PVPh/PMMA/PEO ternary polymer blends

PVPh/PMMA/PEO (wt%)	T_g (°C)	T_m (°C)
100/0/0	150	
0/100/0	105	
0/0100	−67	69.2
10/72/18	−28, 123	62.8
10/54/36	8, 114	65.9
10/36/54	–	66.0
10/18/72	–	66.1
30/56/14	31, 98	
30/42/28	15, 112	
30/28/42	−21, 110	62.0
30/14/56	−24, 114	64.1
50/40/10	7, 104	
50/30/20	44, 96	
50/20/30	11	
50/10/40	−24	
70/24/6	138	
70/18/12	102	
70/12/18	21	
70/6/24	18	
80/16/4	138	
80/12/8	137	
80/8/12	98	
80/4/16	84	

4. Conclusions

The PVPh-*r*-PMMA/PEO blending system is completely miscible in an amorphous phase over the entire composition range. On the contrary, the PVPh-*b*-PMMA/PEO blend system shows a closed-looped phase separated region in the phase diagram due to ΔK effects in the ternary polymer blend. FTIR was employed to study the specific interaction at various compositions and various inter and intramolecular hydrogen bonding. Based on the frequency difference ($\Delta\nu$) from both copolymer/PEO blends, the interassociation between hydroxyl in PVPh and ether in PEO is considerably stronger than either the self-association of hydroxyl in PVPh or the interactions between hydroxyl groups in PVPh and carbonyl groups in PMMA. Based on the Painter–Coleman Association Model (PCAM), a value for $K_C = 300$ is obtained in PVPh-*b*-PMMA/PEO blend system at room temperature. This result gives a good agreement between the experimental and theoretical fraction of hydrogen bonded carbonyl groups for the two sets of copolymer/PEO blends based on a fixed volume fractions of PEO ($\Phi_C = 0.2$). Although the relative ratio of interassociation equilibrium constant of PEO to PMMA is larger in PVPh-*b*-PMMA/PEO blend system, the PVPh-*r*-PMMA/PEO blend system has greater $\Delta\nu$ and greater homogeneity at the molecular scale than the PVPh-*b*-PMMA/PEO blend system because of the ΔK effect.

Acknowledgements

This research was financially supported by the National Science Council, Taiwan, Republic of China, under Contract NSC-94-2216-E-009-002.

References

[1] Huglin MB, Rego JM. Polymer 1990;21:1269.
[2] Lee JY, Painter PC, Coleman MM. Macromolecules 1988;21:954.
[3] Meaurio E, Velada JL, Cesteros LC, Katime I. Macromolecules 1996;29:4598.
[4] Dai J, Goh SH, Lee SY, Siow KS. Polymer 1995;35:2174.
[5] Coleman MM, Graf JF, Painter PC. Specific interactions and the miscibility of polymer blends. Lancaster, PA: Technomic Publishing; 1991.
[6] Kambour RP, Bendler JT, Bopp RC. Macromolecules 1983;16:753.
[7] Paul DR, Barlow JW. Polymer 1984;25:487.
[8] Roe RJ, Rigby D. Adv Polym Sci 1987;82:1.
[9] Woo EM, Barlow JW, Paul DR. Polymer 1985;26:763.
[10] Fernandes AC, Barlow JW, Paul DR. J Appl Polym Sci 1986;32:5357.
[11] Fowler ME, Barlow JW, Paul DR. Polymer 1987;28:1177.
[12] ten Brinke G, Karasz FE, MacKnight WJ. Macromolecules 1983;16:1827.
[13] Shiomi T, Karasz FE, MacKnight WJ. Macromolecules 1986;19:2274.
[14] Jo WH, Lee SC. Macromolecules 1990;23:2261.
[15] Isasi JR, Cesteros LC, Katime I. Macromolecules 1994;27:2200.
[16] Lin CL, Chen WC, Liao CS, Su YC, Huang CF, Kuo SW, et al. Macromolecules 2005;38:6435.
[17] Jo WH, Choi K. Macromolecules 1997;30:1509.
[18] Coleman MM, Painter PC. Prog Polym Sci 1995;20:1.
[19] Hong BK, Kim JK, Jo WH, Lee SC. Polymer 1997;38:4373.
[20] Manestrel CL, Bhagwagar DE, Painter PC, Coleman MM, Graf JF. Macromolecules 1992;25:7101.
[21] Jo WH, Kwon YK, Kwon IH. Macromolecules 1991;24:4708.
[22] Jack KS, Whittaker AK. Macromolecules 1997;30:3560.
[23] Kuo SW, Liu WP, Chang FC. Macromol Chem Phys 2005;206:2307.
[24] Dong J, Ozaki Y. Macromolecules 1997;30:286.
[25] Li X, Hsu SL. J Polym Sci, Polym Phys Ed 1984;22:1331.
[26] Ito H, Russell TP, Wignall GD. Macromolecules 1987;20:2213.
[27] Zawada JA, Ylitalo CM, Fuller GG, Colby RH, Long TE. Macromolecules 1992;25:2896.
[28] Wastlund C, Maurer FHJ. Macromolecules 1997;30:5870.
[29] Chen X, An L, Yin J, Sun Z. Macromolecules 1999;32:5905.
[30] Feldstein MM, Shandryuk GA, Kuptsov SA, Plate NA. Polymer 2000;41:5327.
[31] Kuo SW, Chang FC. Macromol Chem Phys 2001;202:3112.
[32] Kuo SW, Huang WJ, Huang CF, Chan SC, Chang FC. Macromolecules 2004;37:4164.
[33] Schmulbach CD, Drago RS. J Phys Chem 1960;64:1956.
[34] Purcell KF, Drago RS. J Am Chem Soc 1968;89:2874.
[35] Moskala EJ, Varnell DF, Coleman MM. Polymer 1985;26:228.
[36] Chintapalli S, Frech R. Macromolecules 1996;29:3499.
[37] Kuo SW, Chang FC. Macromolecules 2001;34:4089.
[38] Moskala EJ, Howe SE, Painter PC, Coleman MM. Macromolecules 1984;17:1671.
[39] Kuo SW, Lin CL, Chang FC. Macromolecules 2002;35:278.
[40] Coleman MM, Xu Y, Painter PC. Macromolecules 1994;27:127.
[41] Painter PC, Veytsman B, Kumar S, Shenoy S, Graf JF, Xu Y, et al. Macromolecules 1997;30:932.
[42] Coleman MM, Painter PC. Macromol Chem Phys 1998;199:1307.
[43] Zhang H, Bhagwagar DE, Graf JF, Painter PC, Coleman MM. Polymer 1994;35:5379.
[44] Kuo SW, Chan SC, Wu HD, Chang FC. Macromolecules 2005;38:4729.